Nanoscale

Rational design of engineered H-ferritin nanoparticles for siRNA delivery across an in vitro BBB model

Journal:	*Nanoscale*
Manuscript ID	NR-ART-11-2021-007880.R1
Article Type:	Paper
Date Submitted by the Author:	03-Mar-2022
Complete List of Authors:	Yuan, Ziwei; Shanghai Jiao Tong University, School of Pharmacy Wang, Bin; Shanghai Jiao Tong University, School of Pharmacy Teng, Yilong; Shanghai Jiao Tong University, Engineering Research Center of Cell & Therapeutic Antibody, Ministry of Education, and School of Pharmacy Ho, William; New Jersey Institute of Technology, Department of Chemical and Materials Engineering Hu, Bin; Shanghai Jiao Tong University, Engineering Research Center of Cell & Therapeutic Antibody, Ministry of Education, and School of Pharmacy Boakye-Yiadom, Kofi Oti ; Shanghai Jiao Tong University - Minhang Campus, Pharmacy Xu, Xiaoyang; New Jersey Institute of Technology, Department of Chemical and Materials Engineering Zhang, Xue-Qing; Shanghai Jiao Tong University, School of Pharmacy

Rational design of engineered H-ferritin nanoparticles with improved siRNA delivery efficacy across an *in vitro* model of mouse blood-brain barrier (BBB)

Ziwei Yuan,[a] Bin Wang,[a] Yilong Teng,[a] William Ho,[b] Bin Hu,[a] Kofi Oti Boakye-Yiadom,[a] Xiaoyang Xu*[b] and Xue-Qing Zhang*[a]

[a]Engineering Research Center of Cell & Therapeutic Antibody, Ministry of Education, and School of Pharmacy, Shanghai Jiao Tong University, 800 Dongchuan Road, Shanghai 200240, PR China

[b]Department of Chemical and Materials Engineering, New Jersey Institute of Technology, Newark, NJ, 07102, USA

*To whom correspondence should be addressed. E-mail address: xiaoyang@njit.edu (X. Xu) and xueqingzhang@sjtu.edu.cn (X.-Q. Zhang)

Abstract

Gene therapy holds tremendous potential for the treatment of incurable brain diseases including Alzheimer's disease (AD), strokes, gliomas, and Parkinson's disease. The main challenge is the lack of effective gene delivery systems traversing the blood-brain barrier (BBB), due to the complex microvessels present in the brain which restrict substances from the circulating blood to pass through. Recently, increasing efforts have been made to develop promising gene carriers for brain-related disease therapies. One such development is the self-

assembled heavy chain ferritin (HFn) nanoparticles (NPs). HFn NPs have a unique hollow spherical structure that can encapsulate nucleic acid drugs (NADs) and specifically bind to cancer cells and BBB endothelial cells (BBB ECs) via interactions with the transferrin receptor 1 (TfR1) overexpressed on their surfaces, which increases the uptake through the BBB. However, the gene-loading capacity of HFn is restricted by its limited interior volume and negatively charged inner surface; therefore, these drawbacks have prompted the demand for strategies to remould the structure of HFn. In this work, we analyzed the three-dimensional (3D) structure of HFn using Chimera software (v 1.14) and developed a class of internally cationic HFn variants (HFn+ NPs) through arginine mutation on the lumenal surface of HFn. These HFn+ NPs presented powerful electrostatic forces in their cavities, and exhibited higher gene encapsulation efficacy than naive HFn. The top-performing candidate, HFn2, effectively delivered siRNA to glioma cells after traversing the BBB and achieved the highest silencing efficacy among HFn+ NPs. Overall, our findings demonstrated that HFn+ NPs obtained by this genetic engineering method provided critical insights into the future development of nucleic acid delivery carriers with BBB-crossing ability.

Keywords: H-ferritin; self-assembling protein nanoparticles; arginine mutation; gene delivery; Blood-Brain Barrier

1. Introduction

The blood-brain barrier (BBB) is a highly structured network of microvessels composed of microvascular endothelial cells with the support of pericytes and astrocytes, maintaining brain homeostasis through selective permeability.[1, 2] In serving this purpose, the dense endothelial structure, significant transendothelial electrical resistance (TEER) and efflux pumps restrict the transport of a majority of exogenous small therapeutic molecules and macromolecules.[3, 4] Therefore, drug delivery to the brain has long posed severe challenges to researchers, and efficient therapeutics need to be urgently developed, as brain diseases are a critical and fatal event.[5] Gene therapy, including small RNAs (e.g., siRNA, mRNA, and miRNA), has long been a research focus due to the remarkable therapeutic effect in virtually any disease.[6] Recently, it has shed new light on the treatment of incurable brain disorders, such as glioblastoma multiforme (GBM).[7] However, since nucleic acid drugs (NADs) are unstable and negatively charged, they tend to be degraded under physiological conditions and have weak cellular internalization, which leads to low transfection efficiency *in vivo*.[8] Hence, there exists a tremendous demand for the development of appropriate delivery vehicles to protect nucleic acids and improve the delivery efficiency across the BBB .[9, 10]

Various developments in generic gene delivery have been reported involving carriers such as adeno-associated viruses (AAVs), lipid nanoparticles (LNPs), cationic polymers, and inorganic nanoparticles (NPs), but there have been little advances in gene delivery across the specialized BBB. Recently, Deverman et al. explored AAV variants for efficient gene delivery to the mouse brain. But theses capsids seemed to be species-specific and their potency for the gene therapy needs to be further studied.[11, 12] Protein

NPs are emerging as a potential solution due to high biocompatibility and unique features which depend on the particular protein.[13-15] In particular, heavy chain ferritin (HFn), can bind specifically to transferrin receptor 1 (TfR1), one of the major receptors expressed on human or rodent BBB endothelial cells (BBB ECs) and cancer cells,[16] making it a promising biological platform for which to build a carrier to traverse the BBB.[8, 17] Due to its inner cavity being 8 nm in diameter,[18] HFn is capable of loading nucleic acids and protecting them from degradation.[19] In addition, HFn possesses a unique pH-mediated biophysical property of self-assembly-disassembly, which contributes to structural stability under neutral physiological conditions and the release of nucleic acids in an acidic intracellular endosome environment.[20, 21]

Naive HFn has a potent capacity for storing metal ions but not nuclei acids due to its negatively charged interior surface.[22-25] Although nucleic acids can be encapsulated into the cavity of unmodified ferritin,[17] the encapsulation efficiency (EE) remains a hurdle. The entrapment of negatively charged nucleic acids depends mainly on the electrostatic interaction between genes and carriers,[26] and nucleic acids hardly bind to the negatively charged internal surface of HFn NPs.[27] The poor gene-loading capacity has become a significant limitation in the applications of HFn.[28, 29] Despite extensive efforts to encapsulate cargo molecules into HFn, such as pH-mediated disassembly and reassembly,[30] denaturing buffer loading strategy[31] and Ca^{2+}-participating self-assembly,[32] enhancing the EE effectively is still elusive. Additionally, multiple functional motifs have been modified on the external surface of HFn via various

chemical or genetic methods, but few attempts have been made to remould the cavity itself.[18, 33]

In this work, we rationally designed a class of de novo internally cationic HFn variants (HFn+ NPs) and predicted their 3D structures and physicochemical properties using Chimera software. Previous studies demonstrated that electrostatic binding interactions provided a strong driving force for the formation of host-guest complexes,[34, 35] and genetic engineering methods could readily introduce additional functionalities to proteins.[36] By introducing arginine mutations on the lumenal surface of HFn through genetic manipulation, we altered the internal surface conformation and the amount of positive charge within HFn NPs. We modulated the negative charges on the inner surface of HFn into positive charges, thereby assisting siRNA encapsulation during NP formation to enhance the EE of HFn NPs.[37, 38] Considering the limited cavity size of HFn, siRNAs, relatively small-sized RNA molecules, were chosen as the cargo molecule. This natural protein which innately traffics through the BBB was successfully transformed into a vehicle for efficient nucleic acid delivery to the brain while preserving its stability, assembly capacity, and bioactivity. At acidic conditions (pH < 3), HFn+ was broken down into subunits, and incubated with siRNA to achieve adsorption. After incubation, the pH was adjusted to 7.4 to facilitate the reformation of nanostructures and siRNA was loaded into the cavity of the reconstituted HFn+ NPs (Scheme 1A). Moreover, HFn+ could traverse the BBB ECs through TfR1-mediated transcytosis and efficiently knock down the expression of target mRNA in GBM cells through TfR1-mediated endocytosis (Scheme 1B), thus showing promise in silencing

genes related to brain tumor progression by RNAi (Scheme 1C). Overall, these redesigned HFn variants will provide an insight into the rational de novo design of versatile protein cages for BBB traversal and effective gene delivery.

2. Materials and methods

2.1 Materials

Plasmid pET-30a (+) was purchased from Hunan Fenghui Biotechnology Co., Ltd. (China). The hFTH gene (HG13217-G) was obtained as a cDNA clone from Sino Biological Inc. (China). FITC and Isopropyl-β-D-thiogalactopyranoside (IPTG) were purchased from Sigma-Aldrich Co., Ltd. (USA). Kanamycin, ammonium sulfate and gelatin were purchased from Shanghai Aladdin Bio-Chem Technology Co., Ltd. (China). Dulbecco's modified Eagle's medium (DMEM), fetal bovine serum (FBS), Trypsin-EDTA, and Penicillin-Streptomycin solution were purchased from Gibco (USA). Akata start (GE, USA) was used to purify the target proteins. siLuc was synthesized by Suzhou Beixin Biotechnology Co., Ltd. (China). Cy5-labeled siRNA was purchased from Shanghai Jima Pharmaceutical Technology Co., Ltd. (China). Rabbit Anti-Claudin 5 antibody (bs-1241R) and Mouse Anti-CD31 antibody (BH0190) were purchased from Beijing Biosynthesis Biotechnology Co., Ltd. (China). LysoTracker Green (C1047S), DAPI (C1002), and Mycoplasma PCR Detection Kit (C0301S) were purchased from Beyotime (Shanghai, China). Unmentioned agents were purchased from Sigma-Aldrich (USA) unless otherwise indicated.

2.2 General cell culture

A HeLa cell line stably expressing both reporter proteins: firefly *Photinus pyralis* and *Renilla reniformis* luciferase (Dual-Luc HeLa).[39] It was obtained from Alnylam Pharmaceuticals, Inc. and was cultured in DMEM medium containing 10% FBS and 600 μg/mL puromycin. Bioluminescent mouse glial cell lines correlated to glioblastoma (Luc-GL261 cells) and immortalized mouse cerebrovascular ECs line (bEnd.3 cells) were obtained from the American Type Culture Collection (ATCC). Luc-GL261 cells were engineered to stably express firefly luciferase alone and were cultured in DMEM medium containing 10% FBS and 1200 μg/ml G418 disulfate salt, while bEnd.3 cells were cultured in DMEM medium containing 10% FBS. All cells used in the study were between passage number 3 and 6. The doubling time of cell culture was estimated from the population size and generally was about 48 h for cell lines and 72 h for primary cells. All cell cultures used in this work were free of mycoplasma contamination as determined by Mycoplasma PCR Detection Kit (Fig. S1).

2.3 Construction of HFn+ expression plasmids

A series of primers containing arginine mutation sites were biosynthesized, and the sequence information was detailed in Table SI. We obtained cationic mutation fragments using primers through an arginine site-directed mutagenesis method. The HFn+ cDNAs were cloned using an overlap and extension PCR method. Each gene clone was ligated into a pET-30a (+) plasmid to yield the expression vectors, pET-HFn/HFn+. The constructed vectors were subsequently transformed into *E. coli* BL21(DE3), and transformants were obtained by kanamycin-resistance selection.

2.4 Biosynthesis of HFn and HFn+ NPs

Briefly, the expression vectors pET-HFn and pET-HFn+ were transformed into *E. coli* BL21(DE3) according to the manufacturer's instructions. A 1 L LB-kanamycin (50 mg/L) culture of both *E. coli* BL21 (DE3)/HFn and *E. coli* BL21 (DE3)/HFn+ was grown at 37°C until OD_{600} reached 0.6-1.0, then induced with 1 mM IPTG and further incubated at 37°C for 12 h. After incubation, *E. coli* cells were harvested by centrifugation at 5000 g for 45 min and the pellets were resuspended in phosphate buffered saline (PBS) buffer (50 mM PO_4^{3-}, 0.15 M NaCl, pH 7.4). Both HFn and HFn+ proteins were lysed by high-pressure homogenization and sonication until the cell lysates were clear, following the centrifugation of lysates at 10000 g for 30 min. After removing cell debris, supernatants of them were heated at 65°C for 20 min and the resultant supernatants of HFn and HFn+ were stored at -20°C until purification.

2.5 Western blotting (WB) analysis

The supernatants of HFn+ lysates after heating were isolated to measure the protein concentration via a bicinchoninic acid (BCA) protein assay kit. The supernatants containing 20 μg of protein were loaded onto a 12% SDS-polyacrylamide gel electrophoresis (SDS-PAGE) at 120 V to perform immunoblotting and then transferred to polyvinylidene fluoride (PVDF) membranes using a standard method. The membranes were blocked using a solution of 5% bovine serum albumin (BSA) in Tris buffer with tween-20 (TBST) for 2 h and incubated with corresponding primary antibodies overnight at 4 °C. After that, the membranes were incubated with HRP-linked second antibodies (1:500) (Proteintech, USA) at room temperature (RT) for 1 h. Pierce ECL WB substrate was used to observe signals.

2.6 Purification of HFn and HFn+ NPs

For HFn, the resultant supernatant was precipitated by ammonium sulfate (520 g/L) and the precipitate was collected by centrifugation at 22000 g for 45 min. Then it was dissolved in PBS buffer. After dialyzing out the ammonium sulfate, DNase I and RNase A (Sigma Aldrich) were added to a final concentration of 60 μg/mL and 100 μg/mL, respectively, and incubated for 30 min at 37°C. The resultant supernatant was purified by size exclusion chromatography (SEC) on a Superdex 200 PG XK 16/ 100 column (GE Healthcare, USA). The typical yield of HFn was 300 mg per 1 L patch.

As HFn+ with His-tag were capable of loading endogenous RNA molecules during the expression in *E. coli*, optimized protocols were developed to isolate the empty cage in good purity. These involved using a high ionic strength buffer to weaken the interaction with nucleic acids and extended incubation with DNase I and RNase A. Each cell pellet from 1 L culture was resuspended in 50 mL of lysis buffer (50 mM PO_4^{3-}, 0.15 M NaCl, pH 7.4) supplemented with lysozyme (1 mg/mL), DNase I (10 U/mL), RNase A (5 U/mL), and protease inhibitor cocktail (Sigma). Then the lysates were incubated at 37°C for 1 h. After lysis of high-pressure homogenization, sonication, thermal treatment, and centrifugation (10000 g) for 30 min, the supernatant was loaded onto the HisTrap™ HP Column (GE Healthcare, USA). The column was washed with a stepwise imidazole gradient to remove the contaminants and then the target protein was eluted with elution buffer (50 mM PBS, 0.15 M NaCl, 500 mM imidazole, pH 7.4). Purified HFn2 and HFn4 in the different imidazole concentrations of elution buffers were determined qualitatively by WB analysis. After the primary purification, they were

incubated for 0.5 h at 37°C to digest any contaminant *E. coli* RNA which was not removed during the HisTrap™ column purification. The proteins were then ready for SEC and the final purified product was collected and washed several times with the PBS storage buffer using an Amicon filter (MWCO=100 kDa, Millipore). Like before, the final productivity of HFn+ was measured by the BCA protein assay kit. It should be noted that all storage of the proteins and experiments were carried out at RT unless specified otherwise.

2.7 Preparation and characterization of HFn and HFn+

The yielded HFn and HFn+ NPs were characterized using transmission electron microscope (TEM, Thermo Scientific Talos, USA) for morphology analysis and dynamic light scattering (DLS, Malvern, USA) for mean particle size and zeta potential characterization. The purity of protein products was analyzed using 12% SDS-PAGE. The final protein concentrations were determined by UV-vis absorbance at 562 nm by BCA protein assay kit (Beyotime). The stability of the HFn and HFn+ were evaluated by native polyacrylamide gel electrophoresis (Native PAGE).

2.8 Cy5-siRNA encapsulation in HFn+ NPs

Ferritin can break down into subunits under a certain acid or alkaline condition and reassembly when pH is adjusted to physiological conditions.[40-42] In this study, the encapsulation of Cy5-siRNA into HFn+ was achieved via a pH-mediated disassembly/assembly method.[32] The dissociation of HFn+ into discrete subunits was achieved by lowering the pH to 2.0 with HCl. Meanwhile, Cy5-siRNA was added into the disassembled HFn+ solution, and the molar ratio of Cy5-siRNA/protein was chosen

as 1: 8 because it was reported to be the optimal molar ratio for HFn to deliver siRNA.[17, 28] After co-incubation for 20 min, the mixture was adjusted to about pH 7.4 with NaOH and then stirred for another 2 h at room temperature. The reassembled NPs were treated with 3 mg/mL of RNase A at 37°C for 30 min, followed by treatment with 5 mg/mL of proteinase K at 37°C for 30 min. The unwrapped free siRNA outside of HFn/HFn+ was digested by RNase A and proteinase K degraded the RNase A. To demonstrate the successful loading of Cy5-siRNA, 2% agarose gel electrophoresis (AGE) was carried out. The bands of Cy5-siRNA and siRNA@HFn+ NPs were visualized using an ultraviolet imager.

2.9 Encapsulation efficiency (EE) of the Cy5-siRNA@HFn/HFn+ NPs

To calculate the EE of siRNA@HFn/HFn+, Cy5-siRNA was used as a locator to evaluate quantitatively. Cy5-siRNA@HFn/HFn+ NPs were prepared using the previous method at the molar ratios of 1:1, 1:3, 1:5, 1:8, 1:10, and 1:15. The free unencapsulated siRNA was removed with an Amicon filter (MWCO=100 kDa, Millipore). Then the pH of NPs was adjusted to 2.0 using HCl, and the fluorescence intensity of Cy5 was detected after 15 min. The EE was calculated by the following formula: EE (%) = C_t/ $C_{total} \times 100$ (C_t is the concentration of the Cy5-siRNA released from NPs and C_{total} represents the concentration of the total added Cy5-siRNA in the NPs.) Moreover, the disassembled NPs at pH 2.0 were immediately analyzed using 2% AGE and subsequently imaged.

2.10 RNase resistance and NPs stability

The main factor hindering effective siRNA delivery *in vivo* is enzymatic degradation.[43] To evaluate the protective effect of the HFn+ on siRNA, Cy5-siRNA@HFn/HFn+ NPs, were treated with RNase A (5 μL, 3 mg/mL) for different time intervals (0, 4, 8, 16, and 24 h) and the digestion of RNase A was aborted like before. The 2% AGE was run to verify its protection. The rest of the NPs after 24 h of RNase digestion, were stored at 4°C for 4 weeks. Then the same amount of naked siRNA (500 ng) was used as control. To check the serum stability of NPs, samples were incubated with serum-containing medium (10% FBS, pH=7.4) for different durations. In these experiments, the gel was run at 110 V for 20 min and subsequently imaged via an ultraviolet imager.

2.11 *In vitro* release of siRNA from the NPs

For the assessment of the release kinetics, Cy5-siRNA was encapsulated into the HFn, HFn2 and HFn4 NPs. A suspension of Cy5-siRNA@NPs in PBS with either pH 5.0 or pH 7.4 was aliquoted (500 μL) into several semipermeable minidialysis tubes (molecular mass cutoff of 100 kDa; Pierce) and incubated with gentle stirring in frequently renewed PBS (pH 5.0 or pH 7.4) at 37°C in the dark. Cumulative release of siRNA was measured at predetermined time points. For siRNA quantification, a standard curve correlating fluorescence with Cy5-siRNA concentration was used to determine the amount of Cy5-siRNA encapsulated within the NPs. The fluorescence intensity was measured by a multimodal plate reader (excitation/emission 633/670 nm; Tecan, Switzerland).

2.12 Assessment of endosomal escape of Cy5-siRNA@NPs

GL261 cells were seeded into 35 mm petri dishes at a density of 2×10^5 cells per dish and incubated for 24 h in 1 ml of 10% FBS-containing DMEM medium until approximately 40%-50% confluence. Cy5-siRNA@HFn, Cy5-siRNA@HFn2, and Cy5-siRNA@HFn4 NPs were then added and incubated with the cells for 2, 4, and 8 h, respectively. The medium was then removed, and the cells were rinsed three times with PBS. DAPI (Beyotime, C1002) was used to stain the nuclei, and LysoTracker Green (Beyotime, C1047S) was used to stain late endosomes. The cells were observed and imaged using a laser scanning confocal microscopy (LSCM, Leica, USA).

2.13 Cell viability assay

The cytotoxicity of HFn and HFn+ to HeLa, GL261, and primary microglial cells was determined by the Cell Counting Kit-8 (CCK-8) assay. Briefly, cells were seeded into a 96-well plate (1×10^4 cells/well) and incubated for 24 h to allow complete attachment. Then, they were treated with HFn and HFn+ NPs at different concentrations. An equal volume of PBS was used for the control group. After different hours of incubation at 37°C, the mixture was replaced with CCK8 reagent-containing complete medium. After 4 h, absorbance at 490 nm of samples (OD_{sample}) was measured using a multimodal plate reader (Tecan, Switzerland). The untreated cells were taken as a negative control ($OD_{control}$). The medium not containing cells and samples was taken as a blank group (OD_{blank}). The relative cell viability was calculated by using the following formula:

$$\text{Cell Viability (\%)} = (OD_{sample}-OD_{blank})/(OD_{control}-OD_{blank}) \times 100$$

2.14 *In vitro* cell uptake studies

Flow cytometry was used for quantitatively investigating the cellular uptake of the Cy5-siRNA@HFn/HFn2/HFn4 NPs. Briefly, HeLa and GL261 cells were seeded into 24-well plates (Corning) at a density of 5×10^4 cells per well for 24 h to reach 80% confluence, and the culture medium was next replaced with the medium containing 1.5 μM and 3 μM Cy5-siRNA@HFn/HFn+ NPs at a ratio of 8:1. Untreated cells were used as a negative control. After another 12 h, single-cell suspensions were prepared by digestion with 0.25% trypsin followed by filtration through a 300-mesh sieve. From each well, 50,000 events were recorded and analyzed immediately using a FACS Calibur flow cytometry system (BD Biosciences, USA).

2.15 *In Vitro* siRNA Transfection

We used siLuc for encapsulation at a molar ratio of siLuc/protein of 1:8. The samples were washed with PBS to remove free siRNA. Dual-Luc HeLa cells were seeded into 96-well plates (1×10^4 cells per well) for 24 h to reach 70%-80% confluency. Cells were then transfected with 1.5 μM siLuc@HFn/HFn+ NPs overnight and replaced with the fresh medium followed by further incubation in the medium for one day. The expression of firefly and *Renilla* luciferase in HeLa cells was determined by Dual-Glo™ Luciferase assay kits. All the transfection experiments were performed in triplicate. Once we screened the optimal HFn variants, we used the higher dose (3.0 μM) as the transfection concentration to further research. Differently, the expression of firefly luciferase in Luc-GL261 cells were detected by Luciferase Assay System protocol. The silencing of siLuc@HFn+ was determined by comparing detected protein

expression levels in treated groups against the untreated control and termed as relative firefly luciferase expression.

2.16 Immunofluorescence of bEnd.3 cells

bEnd.3 cells were seeded at a density of 5×10^4 cells/cm^2 onto the upper chamber of the transwell pre-coated with gelatin (2% w:v) and allowed to grow until 70%-80% confluency. Cells were fixed with 4% paraformaldehyde for 20 min, washed three times with PBS, permeabilized with 0.5% Triton X-100 in PBS for 5 min and then blocked with 3% BSA for 30 min at RT after three washes with PBS. Primary antibodies were incubated for overnight at 4°C under permeabilized conditions: mouse anti-CD31 antibody (Bioss, BH0190, 1:200) and rabbit anti-Claudin 5 antibody (Bioss, bs-1241R, 1:100). The following secondary antibodies were incubated for 60 min at RT in the dark: goat anti-mouse Cy5 (Servicebio, GB27301, 1:400), and goat anti-rabbit AlexaFluor 488 (Servicebio, GB25303, 1:200). The nuclei were counterstained by incubating with DAPI (Beyotime, C1002, 5 μg/μl) for 10 min. For imaging, laser scanning confocal microscopy (LSCM, Leica, USA) was used.

2.17 *In Vitro* BBB model construction and Transcytosis Assay

The immortalized mouse brain capillary ECs, bEnd.3 cells, were used to generate an *in vitro* BBB model as previously reported.[44] Briefly, bEnd.3 cells were grown on the transwell pre-coated with gelatin (2% w:v) and cultured with DMEM medium containing 10% FBS as described before. The integrity of the cell monolayer was evaluated by measuring the TEER values using a Millicell-ERS Volt-Ohm Meter (Millipore, USA). When TEER reached higher than 200 Ω·cm^2, FITC-labeled

HFn/HFn+ (3 μM) in fresh culture media was added to the apical chamber, and samples from the basal chamber were collected after 2-4 h. FITC fluorescence intensities (490 nm excitation and 525 nm emission) of each aliquot were measured using a multimodal plate reader (Tecan, Switzerland). The relative transcytosis ratio to HFn (%) was defined as the accumulated FITC fluorescence of FITC-HFn+ to that of FITC-HFn when crossing the BBB monolayer.

2.18 Native polyacrylamide gel electrophoresis (Native PAGE)

The integrity of the FITC-HFn+ NPs collected from the basal chamber was also analyzed by Native PAGE (PAGE, 5 % polyacrylamide gels) using freshly prepared FITC-HFn NPs as control.

2.19 Transport across the BBB and knock down luciferase mRNA of glioma cells

BBB co-culture model *in vitro* was established to evaluate the penetrating and traversing effects of HFn/HFn+. Like before, bEnd.3 cells were seeded on 24-well cell culture at a density of 5×10^4 cells per inserted transwell, and then the TEER was measured until it reached 200 $\Omega\cdot cm^2$. Luc-GL261 cells were seeded into another 24-well plate at a density of 5×10^4 cells/well and the bEnd.3 monolayers covered with cell culture were transferred to the plates containing Luc-GL261 cells. After further co-culture for 12 h, siLuc@HFn, siLuc@HFn2, and siLuc@HFn4 (3.0 μM) were added on the apical side, and their luciferase knockdown efficiency was measured after 24 h by a luciferase assay system protocol as shown before. The knockout rate relative to HFn (%) was determined after transcytosis.

2.20 Statistical analysis

All data from at least three independent experiments were presented as mean ± standard deviation (SD). The differences between groups were analyzed using Student's test or one-way analysis of variance (ANOVA). In all cases, ***p***-Values less than 0.05 were considered statistically significance (****p*<0.05, *****p*< 0.01, ******p*< 0.001, *******p*< 0.0001).

3. Results and discussion

3.1 Arginine mutation strategy for HFn+ NPs

A previous study demonstrated that introducing six arginine mutation sites into the inner strands of the O3-33 protein cage could provide a highly positive charge in the lumen.[45] The idea of an attempt to alter inner surface charges of HFn prompted us to select more than six evenly dispersed negatively charged amino acids for the structural mutation to achieve a similar positively charged interior. Rapid advances in computational biology enabled us to have access to the Protein Data Bank (PDB) identification number (ID) of HFn readily.[46] Using Chimera software, we found all the negatively charged amino acids on the inner surface of the HFn protein structure. Eight residues on the inner surface of the HFn monomer (Asp42, Glu61, Glu64, Glu67, Asp131, Glu134, Asn139, and Asp171) were selectively replaced with arginine through site-directed mutagenesis to create a class of HFn+ NPs (Table 1), which were expected to have high affinity for anionic siRNAs via electrostatic binding. As Chimera showed, a complete 3D morphology of HFn consisted of 24 subunits that can self-assemble into a hollow globular structure with 4-3-2 symmetry (Fig. 1A).[36] The positive and negative

charge distributions and the structure of the HFn monomer, were illustrated in Figs. 1B and 1C, respectively. Obviously, all positive charges didn't offset the negative charges and there were more negative charges on the inner surface of subunits.[47] The HFn subunit consists of five helices, a, b, c, d, and e: four long α-helices (a, b, c, and d) and one tilted short helix (e) connected by a short loop. The 3D model revealed that helices c, d, and e were present at the inner strands of HFn while helices a and b were present at the outer strands. Chimera images presented the subunits of six different types of HFn+, termed HFn1, HFn2, HFn3, HFn4, HFn5, and HFn6 (Fig. 1D). We used a computational protein engineering method to simulate the 3D steric structure model of each HFn+. Simulation results for each protein cage along the fourfold symmetry axis, triple symmetry axis, and superficial three-dimensional structure were shown in Fig. 1E to Fig. 1K, respectively. We managed to introduce arginine into the cavity of naive HFn by mutation-induced alteration of the inner surface charge density, which was likely to adjust the binding affinity for siRNA.

In addition, the SIB Bioinformatics Resource Portal tool was used to predict the isoelectric point (pI) of proteins, and the prediction results demonstrated that the theoretical pI values of HFn+ variants (pI=7.42~8.92) were higher than that of HFn (pI=5.30). This significant difference facilitated the encapsulation of siRNA as the interior surface of HFn+ remained positively charged during the process of disassembly and reassembly, thus providing an electrostatic force to promote gene encapsulation (Table 1).

3.2 Preparation and characterization of HFn+ NPs

Building on the computer structural simulation, we identified eight mutation residues and chose six HFn variants with different mutation levels for further study. They were all expressed in *Escherichia coli* (BL21(DE3)) as previously described.[48, 49] With slight modification and optimization during plasmid construction, we fused a 6× His-tag to the N-terminus of HFn for HisTrap™ purification, followed by SEC methods, which ensured the high purity of these HFn+ NPs. Their expression and purity were well verified through WB and SDS-PAGE analysis (Fig. 2A). Herein, with normalization of the total protein amount, the WB results demonstrated that the expression of HFn1 was almost absent; thus, HFn1 was excluded from further screening. In contrast, the other five HFn+ variants were clearly observed to have different levels of expression (Fig. 2B). ImageJ was used to compare the production level of each HFn+ protein semiquantitatively. It is obvious that HFn2 and HFn4 exhibited the higher yield among HFn variants (Fig. 2C). Once we validated the morphology, encapsulation, and biological activity of HFn2 and HFn4, we would assess the remaining three proteins.

A clear single HFn+ protein subunit band was shown at approximately 21 kDa, which was slightly heavier than the molecular weight of HFn, indicative of successful purification (Fig. 2D, Figs. S2, S3, S4, and S5). Up to 90% purity of HFn+ was achieved according to the ImageJ analysis. Moreover, the BCA assay results showed that purified HFn2 and HFn4 had high yields of approximately 80 mg and 55 mg per litre, respectively. TEM morphology showed the homogenous hollow spherical cage-like structures of purified HFn+ NPs, suggesting that the mutant proteins retained their

unique assembly properties (Fig. 2E and Fig. S6). As evidenced by dynamic light scattering (DLS), HFn+ NPs exhibited a negligible change in average size after mutation (Figs. 2F and 3A). The particle size distribution of 12~18 nm indicated that HFn+ was correctly folded and retained many properties similar to HFn, such as self-assembly, stability, nontoxicity, and transcytosis.

3.3 Preparation and characterization of siRNA@HFn or HFn+ NPs

In addition to the verified structural integrity and high purity of HFn+, HFn+ NPs were required to have enough space and flexibility to encapsulate macromolecular NADs. Zhang et al.[40] demonstrated that ferritin is rigid under physiological conditions, but turns to a flexible structure when the pH is adjusted to 2~3. siRNA was predicted to be loaded into the cavity of HFn+ NPs through a pH-mediated disassembly-reassembly procedure to obtain siRNA@HFn+ NPs. The zeta potentials of the HFn, HFn2, HFn3, HFn4, HFn5, and HFn6 NPs were measured with almost no difference under physiological pH (-9.15 mV ~ -10.39 mV). At pH 5, which is similar to the pH of the weakly acidic tumor microenvironment (TME),[50] their zeta potential showed negative charge. This result revealed that HFn+ NPs retained their intact nanostructures when entering the cytoplasm. After pH was adjusted to 2, the nanostructure was broken down into discrete subunits and the overall charge was positive (Fig. 3B). Additionally, the zeta potential of all HFn+ NPs (15.13 mV ~ 22.17 mV) was significantly higher than that of HFn (4.84 mV), likely due to the introduction of positively charged arginine inside the inner surface of HFn+ NPs.

To further investigate the formation of their nano-formulations and EE, Cy5-siRNA was chosen as a locator in the process. After removing the unencapsulated RNA by a filter with a molecular cutoff of 100 kDa, we adjusted the pH to 2.0 to disassemble Cy5-siRNA@HFn and Cy5-siRNA@HFn+ into discrete subunits, and Cy5-siRNA was released from the NPs in the same position as the naked Cy5-siRNA (Fig. 3C). AGE was used to monitor the siRNA of NP-siRNA at a series of siRNA/Protein ratios, from 1:1 to 1:15. The shift of the siRNA location in the gel after being loaded onto NPs showed that maximum encapsulation of siRNAs was achieved when NPs and siRNAs were at the siRNA/Protein ratio of 1:15. Moreover, the EE (%) of HFn and HFn+ loaded with Cy5-siRNA at pH 2 was detected according to the fluorescence intensity of Cy5. Cy5-siRNA@HFn+ (10.10%~52.83%) possessed a significantly higher EE than HFn (6.28%~23.96%). A further increase of the siRNA/Protein ratio to 1:8 enhanced siRNA encapsulation by at least 2.3 times, significantly outperforming naive HFn (Table 2). With increasing molar ratios of HFn/HFn+ to siRNA, EE was observed to increase gradually in a dose-dependent manner. Since no significant EE increase was detected when the siRNA/Protein ratio was between 1:8 and 1:15, the final NP-siRNA was constructed at the siRNA/Protein ratio of 1:8.

To evaluate the protective effect of NPs on siRNA, the enzymatic degradation assay of the NPs was conducted at a Cy5-siRNA/Protein molar ratio of 1:8, and naked siRNA or NP-siRNA was incubated with RNase for different time intervals, followed by 2% AGE. It was confirmed that HFn+ could prevent the enzymatic degradation of nucleic acids and successfully encapsulate siRNA (Fig. 3D). After incubation with

RNase A for 0~24 h, the *in vitro* stability of siRNA in the NPs was examined to investigate their resistance to enzymatic degradation. Even after 24 h of incubation with RNase, most siRNAs were still preserved in NP-siRNA as before (Fig. 3E). Then we stored samples in solution at 4°C for 4 weeks before degrading the RNase with proteinase K. There was no significant decrease in the brightness of the Cy5-siRNA@HFn/HFn+ NP bands after 2% AGE detection (Fig. 3F). *In vitro* serum stability of NPs was tested at 37°C after 24 h of co-incubation. There was no leakage or degradation of siRNA in the NP-siRNA (Fig. 3G). Hence, the siRNA@HFn and siRNA@HFn+ NPs were found to successfully encapsulate siRNA while also protecting it from RNase A degradation.

We monitored release profiles of Cy5-siRNA from different NPs at acidic and neutral conditions. Over a 92-h period of incubation under physiological condition (PBS, pH=7.4), less than 20% Cy5-siRNA was released from HFn, HFn2 or HFn4 NPs, indicating that NPs are sufficiently stable while transporting through the systemic circulation. Under acidic conditions, HFn has been reported to disassemble into protein subunits and release the encapsulated molecules.[51] As shown in Fig. 4A, NPs showed an initial rapid release of Cy5-siRNA and reached a maximum release of 86 ± 3% Cy5-siRNA at 92 h. Compared with HFn NPs, HFn2 and HFn4 NPs showed a slightly slower release at early time points, which is likely due to the internal positive charges in the engineered HFn+ NPs. All NPs reached a plateau and presented a similar release profile after 20 h of incubation. Overall, these findings confirmed the pH-dependent kinetics of siRNA release of the developed HFn+ NPs .

3.4 *In vitro* cytotoxicity evaluation

The safety of delivery systems is of paramount importance to minimize dose-limiting toxicity before clinical studies.[37] We performed safety tests of HFn+ on HeLa, GL261 cell lines and primary microglial cells. To determine the safe dose range of HFn+ NPs for the following transfection assays, HeLa and GL261 cancer cells were treated with HFn2 and HFn4 NPs at different concentrations, and the cell survival rate was analyzed using CCK-8 assay. The cytotoxicity of HFn2 and HFn4 at concentrations ranging from 0.015 μM ~ 6.6 μM was detected after co-incubation with the HeLa cells for 6 h, 12 h, and 24 h (Figs. S7A, S7B and S8). The 3.0 μM cage had no significant toxicity after 12 h of incubation. However, given that they showed toxicity to HeLa cells under certain conditions (3.0 μM or 6.6 μM, 24 h), we preliminarily identified 3.0 μM as the tolerance dose when co-incubated with HeLa or GL261 cells for 12 h, which can cause the minimal toxicity without compromising the transfection efficiency. The cytotoxicity assay results of HFn2 and HFn4 in GL261 cells after 12 h at the same concentration range (0.015-3.0 μM) confirmed our hypothesis, revealing that this transfection condition (3.0 μM, 12 h) was suitable to GL261 cells (Fig. S7C). After 12 h of co-incubation, the cytotoxicity of the other three HFn+ proteins (HFn3, HFn5, HFn6) in both HeLa and GL261 cells was measured at a concentration of 3.0 μM, confirming that the functionalization of arginine in the interior cavity of HFn had no significant toxicity up to 3.0 μM cage in either cell (Fig. S7D). To further conclusively demonstrate the toxicity, we also tested the toxicity of NPs using primary microglial

cells in the concentration range of 0 μM ~ 4 μM, NPs didn't show significant toxicity below 3.0 μM after co-incubation for 12 h (Fig. S9).

3.5 Quantitative cellular uptake of siRNA@HFn+ NPs

We next examined whether arginine mutation could contribute to more efficient cellular uptake of HFn NPs. Flow cytometry was used to evaluate the cellular internalization of Cy5-siRNA@HFn+ NPs in HeLa and GL261 cells. Herein, the cellular uptake of Cy5-siRNA@HFn+ in either cell at a concentration of 1.5 μM was detected in the first round of screening (Fig. S10). Flow cytometry analysis revealed that the cellular mean fluorescence intensity (MFI) of Cy5-siRNA@HFn+ was significantly stronger than the MFI of the control, indicating that more HFn+ NPs were internalized. In addition, we found that GL261 cells took up more Cy5-siRNA@HFn+ than HeLa cells, presumably due to the differences in the expression of TfR1 on these two cells. The NP internalization of all five HFn+ NPs significantly exceeded that of HFn. Among NPs, HFn2, HFn4, and HFn3 were clearly superior to the other variants. Due to the low productivity of HFn3 and its unremarkable cell binding ability, we further investigated the cellular uptake of HFn2 and HFn4 instead of HFn3 in both HeLa and GL261 cells at a higher concentration of 3.0 μM (Figs. 4B and 4C). There were significant fluorescence signal differences in the MFI between HFn+ (HFn2, HFn4) and HFn treated groups while there was no statistical difference between HFn2 and HFn4. Together, these internalization results demonstrated that different positions of HFn where arginine residue mutations occurred may affect the binding affinity to different epitopes on TfR1.[52] HFn2, HFn3, and HFn4 possessed the preferred encapsulation

capability and enhanced cellular uptake, and were promising for the development to facilitate siRNA delivery in the brain. However, considering the drawback of HFn3, we excluded it in the following assays.

3.6 Endosomal escape property

To enable siRNA-mediated gene silencing, NPs need facilitate siRNA escape from endosomes followed with release into the cytoplasm.[10] As shown in Fig. 5A, we observed that Cy5-siRNA@NPs entered GL261 cells rapidly and were partially located in endosomes after 2 h of incubation. The internalized Cy5-siRNA NPs (red) were mainly colocalized with late endosomes (green) at 4 h of incubation, and most of the NPs were located outside of endosomes after another 4 h of incubation, indicating release of the siRNA into the cytoplasm (Fig. 5A). The confocal images demonstrated that HFn2 and HFn4 NPs were able to escape from endosomes after 8 h incubation with GL261 cells.

3.7 *In vitro* gene silencing efficacy of siRNA@HFn+ NPs

It is worthwhile to further investigate the gene silencing efficacy at the cellular level due to their outstanding EE and binding affinity. We evaluated the *in vitro* gene silencing efficacy of siLuc@HFn+ NPs in Dual-Luc HeLa cells and Luc-GL261 cells. Dual-Luc HeLa cells were genetically engineered to stably express both firefly and *Renilla* luciferase, whereas Luc-GL261 cells expressed only firefly luciferase. At the initial screening, 1.5 μM siLuc@HFn+ NPs were incubated with Dual-Luc HeLa cells, and the expression of both reporter proteins was measured after 24 h post-transfection. Significant luciferase knockdown of approximately 50% and 45% were achieved after

treatment with siLuc@HFn2 and siLuc@HFn4 NPs, respectively. In contrast, the siLuc@HFn NPs (~20%) exhibited a significant decrease in the luciferase knock down efficacy (Fig. 5B). The NP-mediated luciferase knockdown was dose-dependent when the loading concentration of luciferase siRNA increased to 3 μM, especially for siLuc@HFn2 and siLuc@HFn4 NPs (Fig. 5C and 5D). No significant fluctuation of Renilla luciferase intensity (internal control) was observed during the down-regulation of luciferase, indicating that HFn2 and HFn4 NPs were not cytotoxic. The difference in gene silencing efficiency of HFn and HFn2 or HFn4 NPs may be partly attributed to the cellular uptake efficiency. These results demonstrated that siRNA@HFn+ NPs had the potential to silence target genes with high efficiency.

3.8 Integrity of *in vitro* BBB model

In vitro BBB model recapitulates a number of characteristics, including the expression of specific endothelial markers and BBB transporter proteins, and the formation of monolayers with high TEER, indicating the presence of tight junctions.[53] *In vitro* models derived from primary cerebral microvessels from various species carried an inherent problem of contamination, slow growth, and de-differentiation. Immortalized mouse brain microvessel endothelial cell lines, bEnd.3 cells, were used to establish an *in vitro* BBB monoculture model since it can express several proteins responsible for the BBB penetration of xenobiotics.[54] In fact, bEnd.3 monocultures have been extensively used to construct *in vitro* BBB models in many published journals.[1, 54-58] Astrocytes and pericytes only provide ~20% of the resistance to various-sized solutes while the endothelium provides ~75–80% of the *in vitro* BBB resistance.[58] Additionally, there is no significant difference between bEnd.3

monoculture model and cocultures comprising mouse brain endothelial cells and astrocytes in terms of many barrier properties (hydraulic conductivity, diffusive solute permeability, etc). At day 4 when the TEER reached 200 $\Omega \cdot cm^2$, we examined the expression of endothelial cell markers and tight junction proteins in the endothelial monolayer. As shown in Fig. 6A, immunostaining of bEnd.3 monolayer showed expression of endothelial cell marker CD31 and provided evidence of cell adhesion, which is consistent with previous reports.[59, 60] Tight junction transmembrane protein claudin-5 expressed on bEnd.3 monolayer indicated the well-formed confluent monolayer on the luminal side of the transwell (Fig. 6B).[61] The immunofluorescence images suggested successful construction of the *in vitro* BBB model that will be used in the following experiments.

3.9 *In vitro* gene silencing effects of HFn+ NPs after traversing the BBB

Due to the higher knockdown efficiency in Luc-GL261 cells, HFn2 and HFn4 emerged as promising vectors for gene delivery to the brain and merited further investigation into their transcytosis ability. We constructed an *in vitro* BBB model using bEnd.3 cells as previously described (Fig. 7A). It was observed that the transcytosis efficiency of HFn2 and HFn4 NPs slightly decreased compared to naïve HFn NPs, but they had no statistical difference (Fig. 7B). Aliquots from the basolateral side of the inserts were collected and tested using Native-PAGE. The bands with a theoretical molecular weight of 504 KDa confirmed that the NPs retained their structural integrity after crossing the BBB monolayer, which is essential for avoiding the undesirable leakage of siRNA that may occur when crossing the BBB (Fig. 7C).

To further study the luciferase knockdown efficiency of HFn2 and HFn4 in Luc-GL261 cells after traversing the BBB, we designed a co-culture model consisting of bEnd.3 cells and Luc-GL261 cells to mimic the TME and BBB (Fig. 7D). As shown in Fig. 7E, despite the lower transcytosis efficiency of HFn2 in comparison with HFn4, its knockdown efficiency increased by 57% compared to HFn and slightly outperformed HFn4. Overall, HFn2 was identified as a promising nanocarrier candidate for siRNA delivery into the brain.

4. Conclusion

In summary, a simple yet elegant electrostatic encapsulation strategy based on an arginine mutation on the inner surface of HFn was adopted which provided a solution to the issue of low siRNA encapsulation and a new modality in which to modify protein cages for therapeutic cargo delivery. HFn2, the optimal HFn variant screened among HFn+ NPs, increased luciferase knockdown efficiency compared to naive HFn after traversing the BBB. Moreover, compared to other HFn+ NPs, HFn2 was readily produced in *E. coli* at a high yield (approximately 80 mg/L with purity up to 90% in this work) and exhibited almost no toxicity. While this nanocarrier still needs to be further explored, optimized, and engineered, our findings revealed that the genetic manipulation of HFn can effectively improve the EE of siRNA, promoting the development of functionalized protein NPs toward BBB-traversing gene delivery.

Author Contributions

Xue-Qing Zhang and Ziwei Yuan conceived the study and designed experiments. Xue-Qing Zhang supervised the research throughout. Ziwei Yuan and Bin Wang carried out the experiments and analyzed the data. Ziwei Yuan and Bin Wang wrote the manuscript. Ziwei Yuan performed all the statistical analysis. Yilong Teng, William Ho, Bin Hu and Kofi Oti Boakye-Yiadom reviewed the manuscript. Xiaoyang Xu and Ziwei Yuan edited and revised the manuscript.

Conflicts of interest

There are no conflicts to declare.

Acknowledgements

The work was funded by the Interdisciplinary Program of Shanghai Jiao Tong University (project number ZH2018ZDA36 (19X190020006)), Shanghai Jiao Tong University Scientific and Technological Innovation Funds (2019TPA10), and the Foundation of National Facility for Translational Medicine (Shanghai) (TMSK-2020-008). Xiaoyang Xu acknowledges support from the American Heart Association (19AIREA34380849), the National Science Foundation (2001606) and the Gustavus and Louise Pfeiffer Research Foundation Award. We thank Xiyun Yan (Institute of Biophysics, CAS) for her generous gift of pET-HFn plasmid and are grateful to Kelong Fan (Institute of Biophysics, CAS) for his professional suggestions on protein purification.

References

1 K. Fan, X. Jia, M. Zhou, K. Wang, J. Conde, J. He, J. Tian and X. Yan, *ACS Nano*, 2018, **12**, 4105-4115.
2 Y. J. Zuchero, X. Chen, N. Bien-Ly, D. Bumbaca, R. K. Tong, X. Gao, S. Zhang, K. Hoyte, W. Luk, M. A. Huntley, L. Phu, C. Tan, D. Kallop, R. M. Weimer, Y. Lu, D. S. Kirkpatrick, J. A. Ernst, B. Chih, M. S. Dennis and R. J. Watts, *Neuron*, 2016, **89**, 70-82.
3 Y. Jiang, J. Zhang, F. Meng and Z. Zhong, *ACS Nano*, 2018, **12**, 11070-11079.
4 N. Weiss, F. Miller, S. Cazaubon and P. O. Couraud, *Biochim Biophys Acta*, 2009, **1788**, 842-857.
5 C. Saraiva, C. Praca, R. Ferreira, T. Santos, L. Ferreira and L. Bernardino, *J Control Release*, 2016, **235**, 34-47.
6 L. Naldini, *Nature*, 2015, **526**, 351-360.
7 D. Kwon, *Nature*, 2021, **592**, 180-183.
8 L. Alvarez-Erviti, Y. Seow, H. Yin, C. Betts, S. Lakhal and M. J. Wood, *Nat Biotechnol*, 2011, **29**, 341-345.
9 S. F. Dowdy, *Nat Biotechnol*, 2017, **35**, 222-229.
10 G. Sahay, W. Querbes, C. Alabi, A. Eltoukhy, S. Sarkar, C. Zurenko, E. Karagiannis, K. Love, D. Chen, R. Zoncu, Y. Buganim, A. Schroeder, R. Langer and D. G. Anderson, *Nat Biotechnol*, 2013, **31**, 653-658.
11 Q. Huang, K. Y. Chan, I. G. Tobey, Y. A. Chan, T. Poterba, C. L. Boutros, A. B. Balazs, R. Daneman, J. M. Bloom, C. Seed and B. E. Deverman, *PLoS One*, 2019, **14**, e0225206.
12 B. E. Deverman, P. L. Pravdo, B. P. Simpson, S. R. Kumar, K. Y. Chan, A. Banerjee, W. L. Wu, B. Yang, N. Huber, S. P. Pasca and V. Gradinaru, *Nat Biotechnol*, 2016, **34**, 204-209.
13 E. J. Lee, N. K. Lee and I. S. Kim, *Adv Drug Deliv Rev*, 2016, **106**, 157-171.
14 M. Uchida, M. T. Klem, M. Allen, P. Suci, M. Flenniken, E. Gillitzer, Z. Varpness, L. O. Liepold, M. Young and T. Douglas, *Advanced Materials*, 2007, **19**, 1025-1042.
15 S. Bhaskar and S. Lim, *NPG Asia Mater*, 2017, **9**, e371.
16 K. Fan, C. Cao, Y. Pan, D. Lu, D. Yang, J. Feng, L. Song, M. Liang and X. Yan, *Nat Nanotechnol*, 2012, **7**, 459-464.
17 L. Li, M. Munoz-Culla, U. Carmona, M. P. Lopez, F. Yang, C. Trigueros, D. Otaegui, L. Zhang and M. Knez, *Biomaterials*, 2016, **98**, 143-151.
18 M. Truffi, L. Fiandra, L. Sorrentino, M. Monieri, F. Corsi and S. Mazzucchelli, *Pharmacol Res*, 2016, **107**, 57-65.
19 J. He, K. Fan and X. Yan, *J Control Release*, 2019, **311-312**, 288-300.
20 M. Bellini, S. Mazzucchelli, E. Galbiati, S. Sommaruga, L. Fiandra, M. Truffi, M. A. Rizzuto, M. Colombo, P. Tortora, F. Corsi and D. Prosperi, *J Control Release*, 2014, **196**, 184-196.
21 B. Jiang, X. Chen, G. Sun, X. Chen and K. Fan, *Nano Today*, 2020, **35**, 100948.
22 B. R. Lee, H. K. Ko, J. H. Ryu, K. Y. Ahn, Y. H. Lee, S. J. Oh, J. H. Na, T. W. Kim, Y. Byun, I. C. Kwon, K. Kim and J. Lee, *Sci Rep*, 2016, **6**, 35182.
23 P. Santambrogio, A. Cozzi, S. Levi, E. Rovida, F. Magni, A. Albertini and P. Arosio, *Protein Expr Purif*, 2000, **19**, 212-218.
24 Lawson, M. D., Artymiuk and J. P., *Nature*, 1991, **349**, 541-541.
25 Kenji, Iwahori, Keiko, Yoshizawa, Masahiro, Muraoka, Ichiro and Yamashita, *Inorganic Chemistry*, 2005, **44**, 6393–6400.
26 T. Beck, S. Tetter, M. Kunzle and D. Hilvert, *Angew Chem Int Ed Engl*, 2015, **54**, 937-940.
27 P. M. Harrison and P. Arosio, *Biochimica et Biophysica Acta*, 1996, **1275**, 161-203.
28 H. Huang, S. Yuan, Z. Ma, P. Ji, X. Ma, Z. Wu and X. Qi, *Biomater Sci*, 2020, **8**, 1759-1770.
29 I. Inoue, M. Chiba, K. Ito, Y. Okamatsu, Y. Suga, Y. Kitahara, Y. Nakahara, Y. Endo, K. Takahashi, U. Tagami and N. Okamoto, *Nanoscale*, 2021, **13**, 1875-1883.
30 Z. Yang, X. Wang, H. Diao, J. Zhang, H. Li, H. Sun and Z. Guo, *Chemical Communications*, 2007, **33**, 3453.

31 M. Liang, K. Fan, M. Zhou, D. Duan, J. Zheng, D. Yang, J. Feng and X. Yan, *Proc Natl Acad Sci U S A*, 2014, **111**, 14900-14905.
32 H. Huang, K. Sha, H. Veroniaina, Z. Wu, Z. Wu and X. Qi, *Nanoscale*, 2020, **12**, 7347-7357.
33 A. E. Powell, K. Zhang, M. Sanyal, S. Tang, P. A. Weidenbacher, S. Li, T. D. Pham, J. E. Pak, W. Chiu and P. S. Kim, *ACS Cent Sci*, 2021, **7**, 183-199.
34 S. Tetter and D. Hilvert, *Angew Chem Int Ed Engl*, 2017, **56**, 14933-14936.
35 R. Zschoche and D. Hilvert, *J Am Chem Soc*, 2015, **137**, 16121-16132.
36 Y. Jin, J. He, K. Fan and X. Yan, *Nanoscale*, 2019, **11**, 12449-12459.
37 M. Kih, E. J. Lee, N. K. Lee, Y. K. Kim, K. E. Lee, C. Jeong, Y. Yang, D. H. Kim and I. S. Kim, *Biomaterials*, 2018, **180**, 67-77.
38 E. J. Lee, G. H. Nam, N. K. Lee, M. Kih, E. Koh, Y. K. Kim, Y. Hong, S. Kim, S. Y. Park, C. Jeong, Y. Yang and I. S. Kim, *Adv Mater*, 2018, **30**, 1705581.
39 None, *Proceedings of the National Academy of Sciences of the United States of America*, 2010, **107**, 9915-9915.
40 S. Zhang, J. Zang, H. Chen, M. Li, C. Xu and G. Zhao, *Small*, 2017, **13**, 1701045.
41 M. Kim, Y. Rho, K. S. Jin, B. Ahn, S. Jung, H. Kim and M. Ree, *Biomacromolecules*, 2011, **12**, 1629-1640.
42 X. T. Ji, H. Lin and H. Q. Huang, *Journal of Proteomics*, 2012, **75**, 3145-3157.
43 S. W. Young, M. Stenzel and J. L. Yang, *Crit Rev Oncol Hematol*, 2016, **98**, 159-169.
44 M. Zhai, Y. Wang, L. Zhang, M. Liang, S. Fu, L. Cui, M. Yang, W. Gong, Z. Li, L. Yu, X. Xie, C. Yang, Y. Yang and C. Gao, *Drug Deliv*, 2018, **25**, 1013-1024.
45 T. G. W. Edwardson, T. Mori and D. Hilvert, *J Am Chem Soc*, 2018, **140**, 10439-10442. W. L. Hsu, C. J. Oldfield, B. Xue, J. Meng, F. Huang, P. Romero, V. N. Uversky and A. K. Dunker, *Protein Sci*, 2013, **22**, 258-273.
46 S. Yin, B. Zhang, J. Lin, Y. Liu, Z. Su and J. Bi, *Eng Life Sci*, 2021, **21**, 630-642.
47 M. Liang, H. Tan, J. Zhou, T. Wang, D. Duan, K. Fan, J. He, D. Cheng, H. Shi, H. S. Choi and X. Yan, *ACS Nano*, 2018, **12**, 9300-9308.
48 Z. Zhen, W. Tang, C. Guo, H. Chen and X. Lin, *ACS Nano*, 2013, **7**, 6988–6996.
49 P. Swietach, R. D. Vaughan-Jones, A. L. Harris and A. Hulikova, *Philosophical Transactions of the Royal Society B: Biological Sciences*, 2014, **369**, 20130099.
50 P. Arosio, R. Ingrassia and P. Cavadini, *Biochimica et Biophysica Acta (BBA) - General Subjects*, 2009, **1790**, 589-599.
51 H. Alonso-Navarro, F. Javier Jimenez-Jimenez, E. Garcia-Martin and J. AG Agundez, *Current drug metabolism*, 2014, **15**, 129-181.
52 R. C. Brown, A. P. Morris and R. G. O'Neil, *Brain Research*, 2007, **1130**, 17-30.
53 Y. Omidi, L. Campbell, J. Barar, D. Connell, S. Akhtar and M. Gumbleton, *Brain Research*, 2003, **990**, 95-112.
54 J. Xue, Z. Zhao, L. Zhang, L. Xue, S. Shen, Y. Wen, Z. Wei, L. Wang, L. Kong, H. Sun, Q. Ping, R. Mo and C. Zhang, *Nat Nanotechnol*, 2017, **12**, 692-700.
55 W. Wan, L. Cao, L. Liu, C. Zhang, B. Kalionis, X. Tai, Y. Li and S. Xia, *J Neurochem*, 2015, **134**, 382-393.
56 C. E. Van Skike, J. B. Jahrling, A. B. Olson, N. L. Sayre, S. A. Hussong, Z. Ungvari, J. D. Lechleiter and V. Galvan, *Am J Physiol Heart Circ Physiol*, 2018, **314**, H693-H703.
57 G. Li, M. J. Simon, L. M. Cancel, Z. D. Shi, X. Ji, J. M. Tarbell, B. Morrison, 3rd and B. M. Fu, *Ann Biomed Eng*, 2010, **38**, 2499-2511.
58 M. M. Salman, G. Marsh, I. Kusters, M. Delince, G. Di Caprio, S. Upadhyayula, G. de Nola, R. Hunt, K. G. Ohashi, T. Gray, F. Shimizu, Y. Sano, T. Kanda, B. Obermeier and T. Kirchhausen, *Front Bioeng Biotechnol*, 2020, **8**, 573775.
59 B. A. Imhof and D. Dunon, *Advances in Immunology*, 1995, **58**, 345-416.
60 N. R. Wevers, D. G. Kasi, T. Gray, K. J. Wilschut, B. Smith, R. van Vught, F. Shimizu, Y. Sano, T. Kanda, G. Marsh, S. J. Trietsch, P. Vulto, H. L. Lanz and B. Obermeier, *Fluids Barriers CNS*, 2018, **15**, 23.

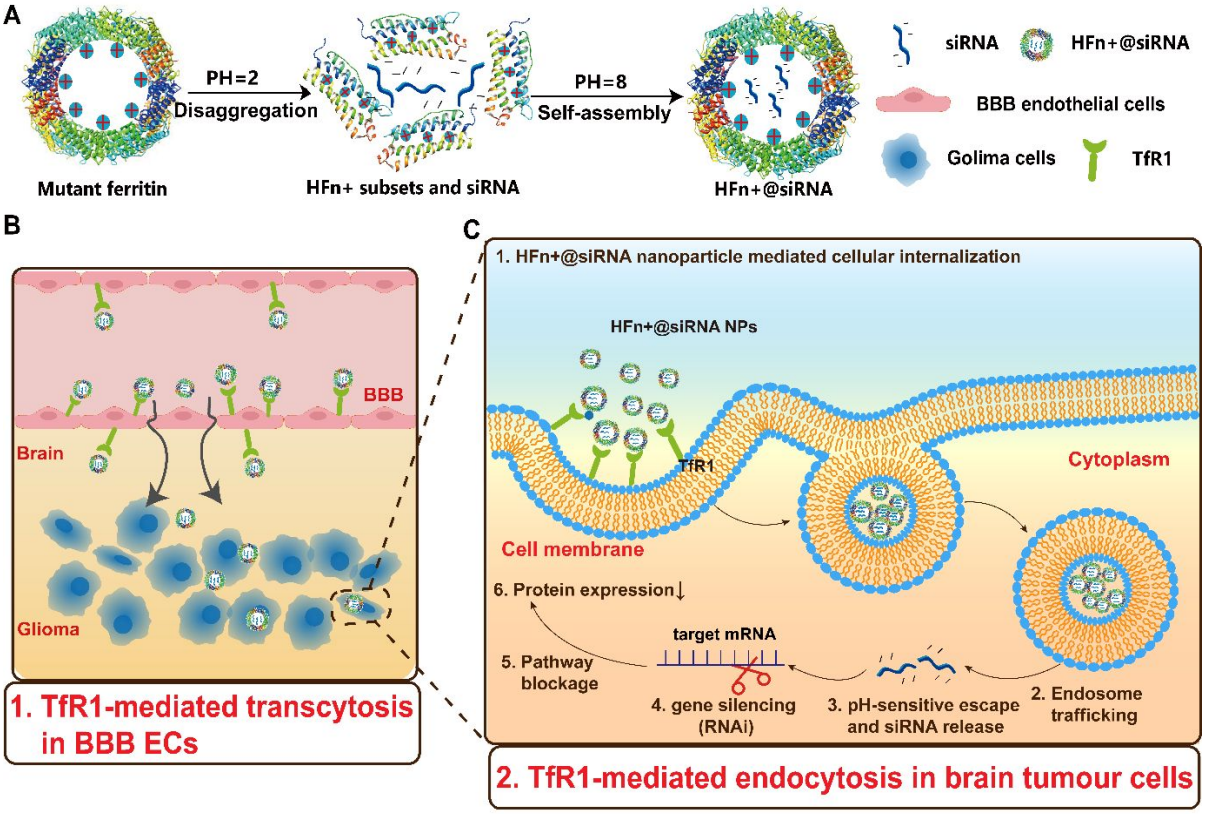

Scheme 1 Schematic illustration of HFn+ NPs-mediated siRNA delivery for regulating brain tumor progression. (A) 3D model of the HFn+ subunit and self-assembled HFn+ NPs, generated using Chimera simulation software. These HFn+ NPs encapsulated siRNA using an assembly/disassembly method. (B) The siRNA@HFn+ NPs traverse the BBB through TfR1-mediated transcytosis and target glioma cells via TfR1-mediated endocytosis. (C) Following the cellular uptake of siRNA@HFn+, siRNA released from the endosomes interferes with protein expression levels via RNAi and has the potential to block brain cancer-related pathways for disease therapy.

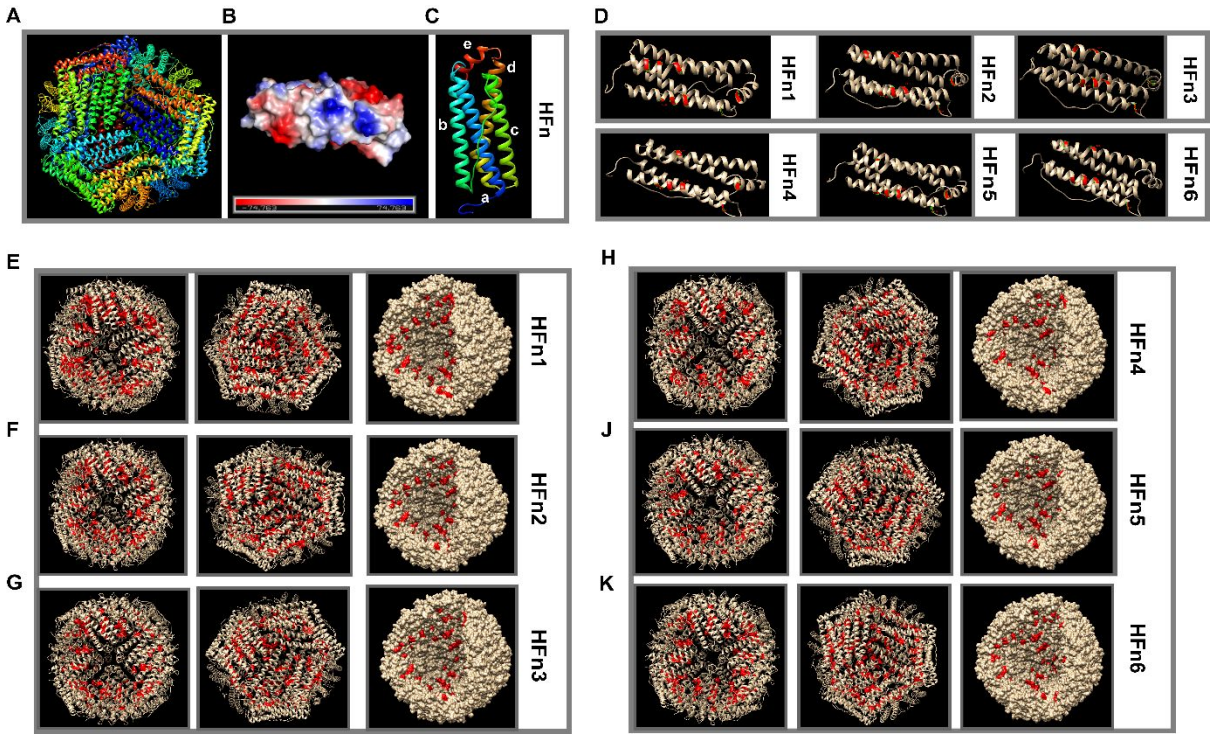

Fig. 1 Design of the supercharged HFn NPs. (A) Wild-type HFn (PDB ID: 3AJO) with 24 monomers displayed in different colors. (B) The charge distribution of the HFn subunit and (C) the structure of the HFn subunit (five helixes from the NH2- and COOH-termini are labelled a, b, c, d, and e, respectively) were generated using Chimera simulation software. (D) The arginine mutation sites on the inner surface of HFn subunits (gray) are highlighted in red by Chimera, demonstrating the different types of mutations of the HFn subunit. (E-K) 3D structural models of HFn+ protein NPs surrounding a fourfold and threefold axis are shown in column 1 and column 2. The surface crystal structures of HFn+ NPs are shown in column 3 by computer simulation. Six HFn+ proteins are displayed in total, including HFn1, HFn2, HFn3, HFn4, HFn5, and HFn6. All of the arginine mutation sites are introduced in red.

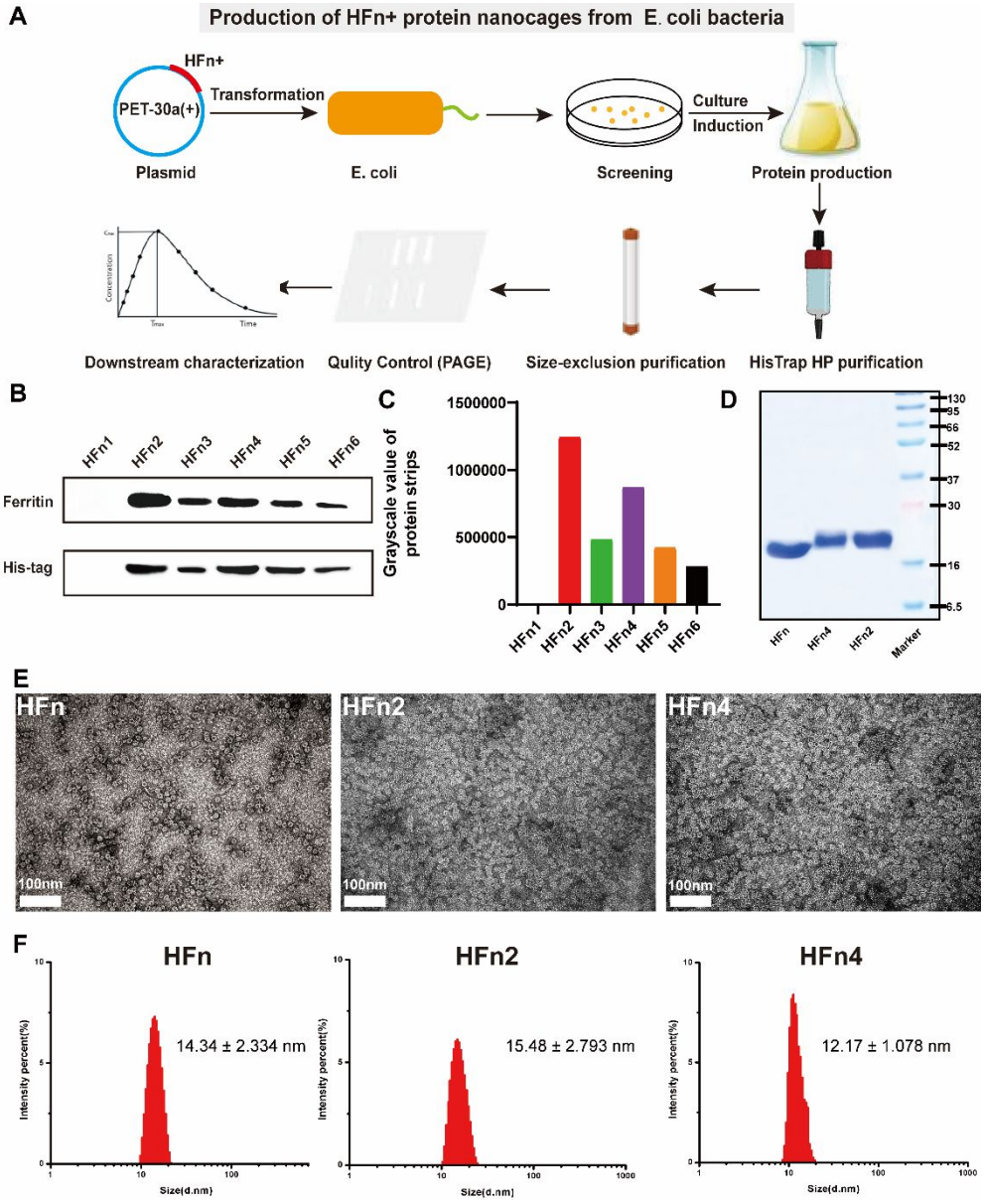

Fig. 2 Preparation, characterization, and encapsulation verification of HFn+ NPs. (A) Scheme for the expression and purification of HFn+ in *E. coli*, and subsequent research on HFn+. (B) The expression of HFn+ and His-tag from HFn+ proteins was evaluated qualitatively by WB detection. (C) Semi-quantitative analysis of the ferritin or His expression levels of HFn+ measured using ImageJ. (D) SDS-PAGE for HFn+ purity analysis. (E) Representative TEM images of HFn, HFn2, and HFn4 NPs. Scale bars: 100 nm (F) DLS analysis of HFn, HFn2, and HFn4 NPs (***n***=3).

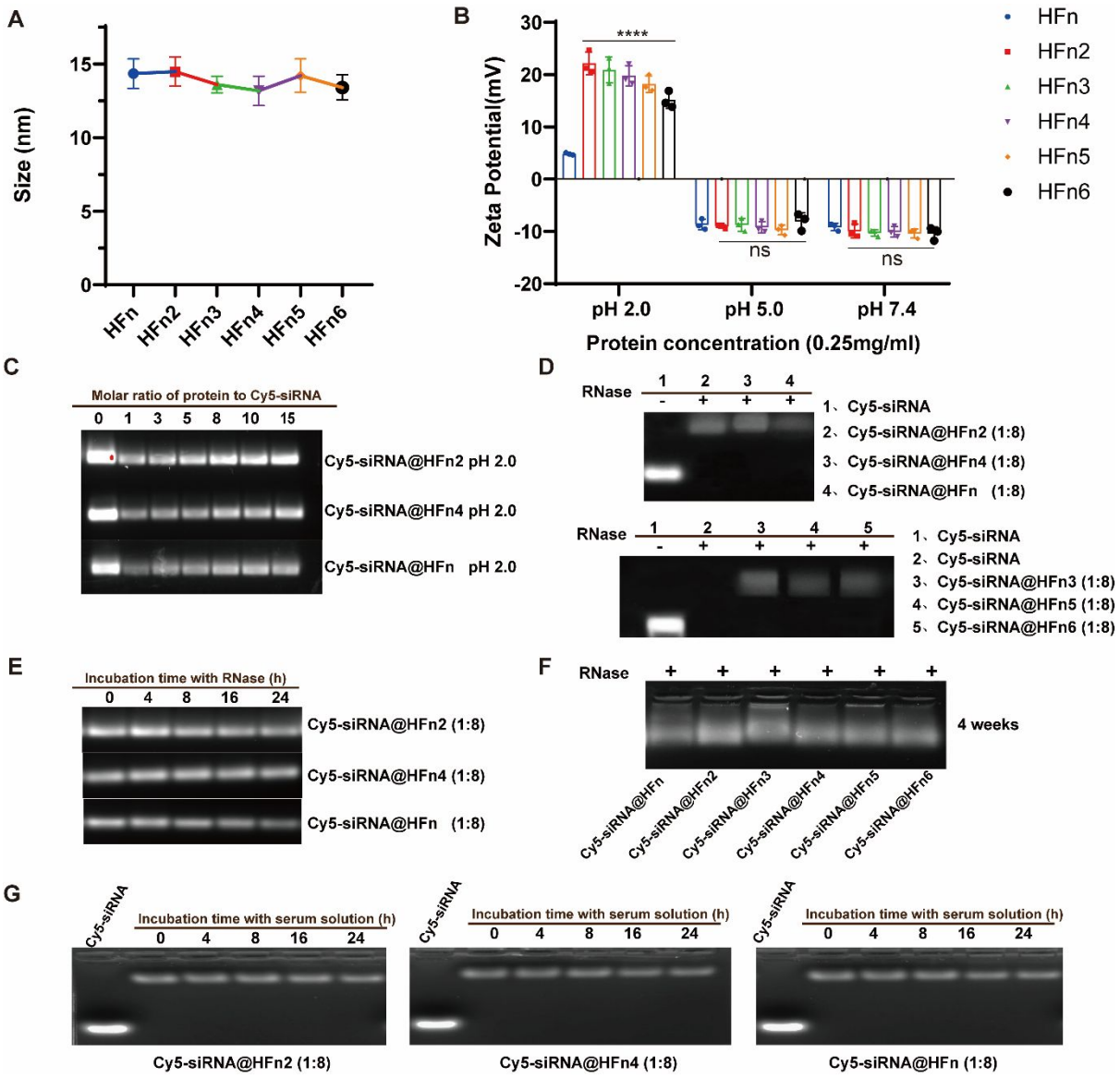

Fig. 3 (A) DLS diameters of HFn and HFn+ (***n***=3). (B) Zeta potential of HFn+ NPs in buffers with pH 7.4, 5.0, and 2.0 (PBS, 0.05 M PO_4^{3-}, 0.15 M NaCl), respectively (***n***=3; ****p < 0.0001 vs. HFn). (C) The 2% agarose electrophoresis results of Cy5-siRNA@HFn2, Cy5-siRNA@HFn4 and Cy5-siRNA@HFn disassembled in pH 2.0 buffers with encapsulation ratios of 1: 1, 1: 3, 1: 5, 1: 8, 1: 10, and 1: 15, respectively. (D) RNase stability of naked siRNA, Cy5-siRNA@HFn+ and Cy5-siRNA@HFn (1: 8) NPs and (E) the co-incubation of HFn2, HFn4 and HFn with RNase A (3 mg/mL) at 37°C for 0, 4, 8, 12, 16, and 24 h were detected by AGE. (F) Stability of all Cy5-siRNA@HFn+ and Cy5-siRNA@HFn (1: 8) NPs

after being stored at 4°C for four weeks, as detected by AGE. (G) Stability of siRNA@HFn, siRNA@HFn2, and siRNA@HFn4 (1:8) NPs in serum-supplemented medium (10% FBS, pH=7.4) at 37°C for 0, 4, 8, 16, and 24 h, as detected by AGE. Significant differences were assessed using a one-way ANOVA with the Turkey test (A and B). Data in (A and B) are presented as mean ± SD from the second repeat.

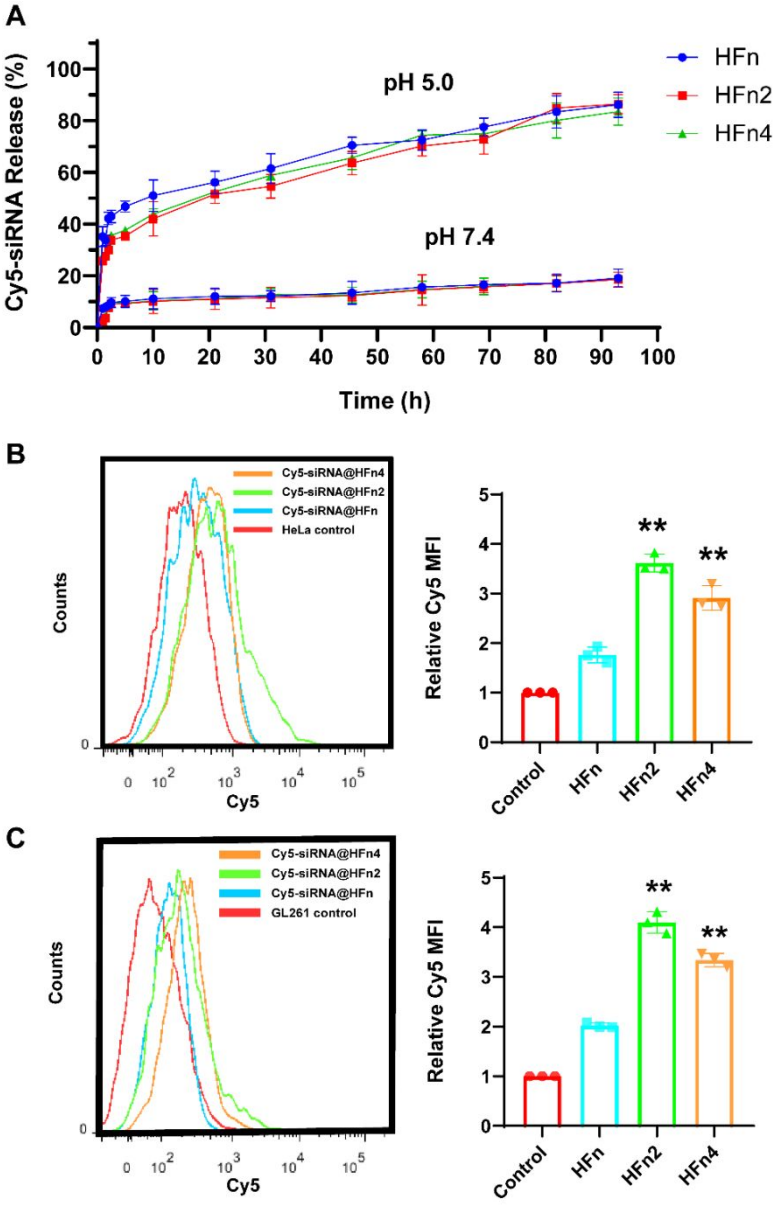

Fig. 4 Cy5-siRNA release kinetics and cellular uptake of Cy5-siRNA@HFn+ NPs in Dual-Luc-HeLa cells and Luc-GL261 cells. (A) *In vitro* release profile of the Cy5-siRNA from HFn, HFn2, and HFn4 NPs at pH 5.0 and pH 7.4 at 37°C (***n***=3, bars represent means ± SD). Flow cytometry analysis of the uptake of Cy5-siRNA@HFn and Cy5-siRNA@HFn+ (Cy5-siRNA@HFn2, Cy5-siRNA@HFn4) in (B) HeLa cells and (C) GL261 cells (***n***=3; ****p* < 0.01 vs. Cy5-siRNA@HFn). Significant differences were assessed using a one-way

ANOVA with the Turkey test (B-C). Data in (B-C) are presented as mean ± SD from the second repeat.

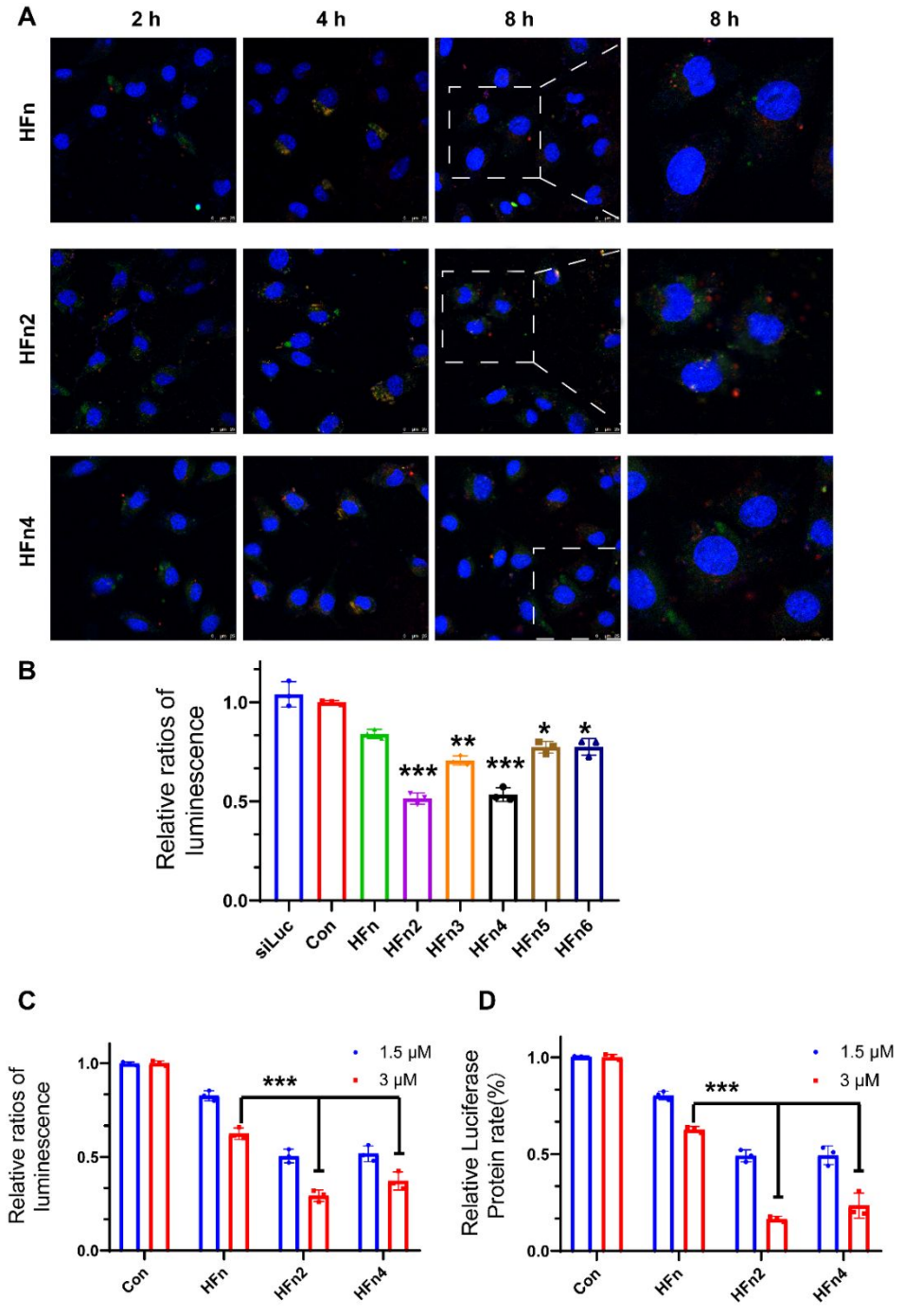

Fig. 5 Endosomal escape capacity of NPs in GL261 cells and gene silencing efficiency in Dual-Luc-HeLa cells and Luc-GL261 cells. (A) Endosome escape of Cy5-siRNA (red)–loaded HFn, HFn2, and HFn4 NPs after incubation with GL261 cells for 2, 4, and

8 h. Nuclei were stained with DAPI (blue), and late endosomes were stained with Lyso-Tracker Green (green). Scale bars: 25 μm. (B) Firefly luminescence ratio in Dual-Luc HeLa cells after transfection with 1.5 μM siLuc@HFn+ NPs at a 1:8 ratio (***n***=3; ****p*** < 0.01 vs. Cy5-siRNA@HFn). (C) Relative firefly luciferase expression in Dual-Luc HeLa cells transfected with siLuc@HFn/HFn2/HFn4 NPs at an elevated dose of NPs (3.0 μM) in a 1:8 ratio (***n***=3). (D) The same dose was used in Luc-GL261 cells (***n***=3; ***p*** < 0.05, ****p*** < 0.01, *****p*** < 0.001 vs. siLuc@HFn). Significant differences were assessed using a one-way ANOVA with the Turkey test (B-D). Data in (B-D) are presented as mean ± SD from the second repeat.

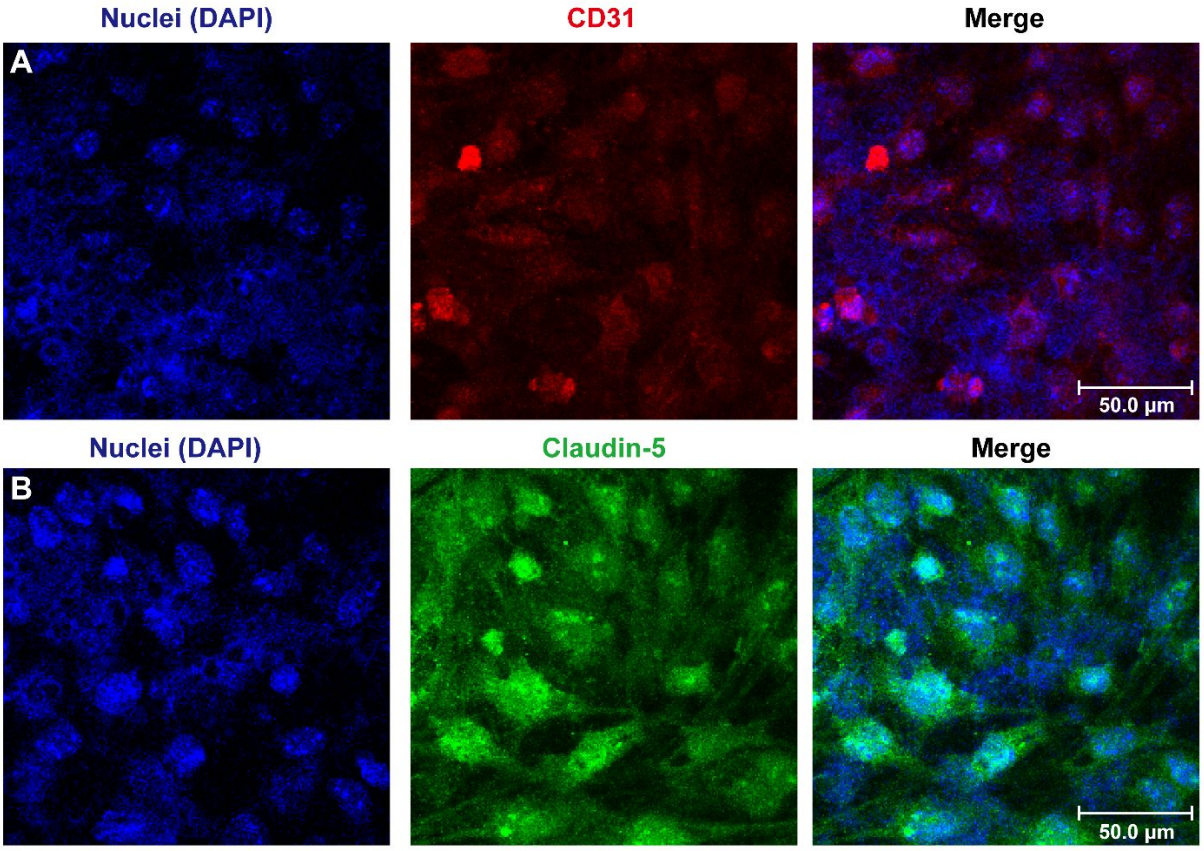

Fig. 6 (A) Immunostaining of a bEnd.3 monolayer for endothelial cell marker CD31 (red). (B) Immunostaining of a bEnd.3 monolayer for tight junction marker claudin-5 (green) and couterstained with cell nucleus dye DAPI (blue). Scale bars: 50 µm

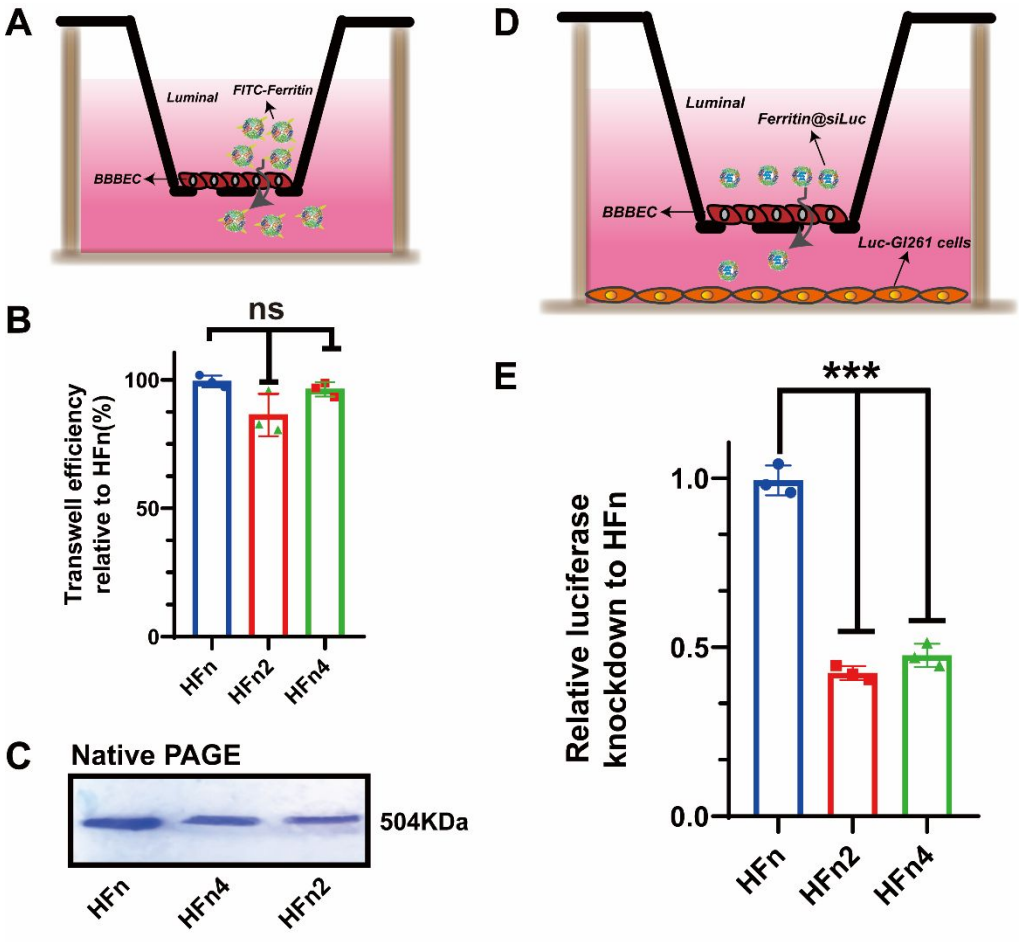

Fig. 7 siLuc@HFn+ NPs successfully traversed the BBB and knocked down luciferase expression while maintaining their structure intact after passing through BBB ECs. (A) Schematic illustration of the *in vitro* BBB model. (B) Transcytosis efficiency of HFn, HFn2, and HFn4 in an *in vitro* BBB model (***n***=3). (C) Native-PAGE analysis of the traversed HFn, HFn2, and HFn4 samples from the basal chamber. (D) Schematic illustration of a co-culture model involving bEnd.3 and Luc-GL261 cells to mimic the BBB and TME. (E) The relative luciferase knockdown efficiency of HFn2 and HFn4 to HFn in cancer cells after traversing the BBB (***n***=3; ***p*** > 0.05 (ns), ***$p < 0.001$ vs. siLuc@HFn). Significant differences were assessed using a one-way ANOVA with the Turkey test (B and E). Data in (B and E) are presented as mean ± SD from the second repeat.

Table 1. The specific arginine mutation sites on the inner surface of HFn and the prediction of the theoretical pI of HFn+

Identity	Number of mutations	Arginine mutation sites	Theoretical value of pI
HFn1	8	D(Asp42), E(Glu61), E(Glu64), E(Glu67), D(Asp131),E(Glu134),N(Asn139),D(Asp171)	8.92
HFn2	7	D(Asp42), E(Glu61), E(Glu64), E(Glu67), D(Asp131), N(Asn139), D(Asp171)	8.71
HFn3	7	D(Asp42), E(Glu61), E(Glu64), E(Glu67), E(Glu134), N(Asn139), D(Asp171)	8.41
HFn4	6	D(Asp42), E(Glu61), E(Glu64), E(Glu67), N(Asn139), D(Asp171)	7.95
HFn5	6	D(Asp42), E(Glu61), E(Glu64), E(Glu67), E(Glu134), D(Asp171)	7.42
HFn6	6	D(Asp42), E(Glu61), E(Glu64), E(Glu67), D(Asp131), N(Asn139)	7.42

Note: The theoretical pI values of HFn+ proteins were calculated using the SIB Bioinformatics Resource Portal tool. (http://web.expasy.org/protparam/).

Table 2. EE (%) evaluation of the Cy5-siRNA@HFn+ NPs with different molar ratios of siRNA/protein at 1:1, 1:3, 1:5, 1:8, 1:10 and 1:15

Molar ratio of siRNA to protein	siRNA@HFn	siRNA@HFn2	siRNA@HFn3	siRNA@HFn4	siRNA@HFn5	siRNA@HFn6
1: 1	6.28±0.65	11.10±2.30	12.01±1.05	13.01±0.86	12.05±1.40	10.10±1.06
1: 3	11.33±0.49*	24.94±4.25*	21.46±3.73**	23.57±2.59**	20.44±2.56*	19.75±2.95*
1: 5	13.63±1. 04*	34.91±2.93***	33.55±1.23**	32.45±0.32***	30.19±1.36**	30.56±0.82**
1: 8	15.72±0.36**	43.77±4.05***	41.64±3.42***	38.74±2.14***	34.97±3.52***	35.74±2.46***
1: 10	17.20±1.11**	45.28±2.47***	43.04±2.33****	40.04±2.33****	37.28±2.47***	38.41±1.63***
1: 15	23.96±2.40**	52.83±4.02***	50.17±3.60****	46.70±3.75****	42.83±3.26***	43.06±3.54****

Note: EE (%) = $C_t/C_{total} \times 100\%$, where C_t is the concentration of the Cy5-siRNA detected by the fluorescence spectrophotometer and C_{total} represents the concentration of the total added Cy5-siRNA in the NPs. *$p < 0.05$, **$p < 0.01$, ***$p < 0.001$, and ****$p < 0.0001$ indicate differences at a molar ratio of 1: 1 (siRNA: protein). Significant differences were assessed using a one-way ANOVA with Turkey test. Data are presented as mean ± SD from the second repeat.